Charge-State Independent Anomalous Transport for a Wide Range of Different Impurity Species Observed at Wendelstein 7-X

A. Langenberg,[1, a)] Th. Wegner,[1] N.A. Pablant,[2] O. Marchuk,[3] B. Geiger,[1] N. Tamura,[4] R. Bussiahn,[1] M. Kubkowska,[5] A. Mollén,[2] P. Traverso,[2] H.M. Smith,[1] G. Fuchert,[1] S. Bozhenkov,[1] H. Damm,[1] E. Pasch,[1] K.-J. Brunner,[1] J. Knauer,[1] M. Beurskens,[1] R. Burhenn,[1] R.C. Wolf,[1] and the W7-X Team[b)]

[1)] *Max-Planck-Institut für Plasmaphysik, 17491 Greifswald, Germany*

[2)] *Princeton Plasma Physics Laboratory, Princeton, NJ 08543, USA*

[3)] *Forschungszentrum Jülich GmbH, Institut für Energie- und Klimaforschung, 52425 Jülich, Germany*

[4)] *National Institute for Fusion Science, Gifu 509-5292, Japan*

[5)] *Institute of Plasma Physics and Laser Microfusion, 01-497 Warsaw, Poland*

(Dated: 22 April 2020)

In this paper, the plasma volume averaged impurity confinement of selected charge states and impurity species has been characterized for the stellarator Wendelstein 7-X (W7-X), covering a wide range of atomic charges (Z=12-44) and atomic masses (M=28-184). A comparison of the experimental findings to theoretical neoclassical and turbulent transport expectations suggests, beside the neoclassical transport, an additional significant anomalous transport mechanism, that is not inconsistent with the predictions of a turbulence dominated impurity transport and is in agreement with experimental results from recent transport studies based on direct measurements of impurity diffusion profiles, performed at W7-X.

PACS numbers: Valid PACS appear here

I. INTRODUCTION

The presence of impurities in the plasma can have a significant impact on the overall plasma properties, including aspects of improved but also of degraded plasma performance. Typical examples are power exhaust[1,2] or edge localized modes buffering[3] by impurity seeding on the one hand but also *e.g.* undesired plasma termination events[4,5] on the other hand. In the latter case, particular high Z materials may cause radiative collapses due to dissipative radiative transitions of non fully ionized impurities, especially critical in combination with impurity accumulation scenarios[5,6]. As the divertor and other plasma facing components, being the main edge impurity sources in fusion devices, are designed using low as well as high Z materials like C[7], Fe[8], or W[9], a comparative experimental determination of the transport properties of different impurity species from low to high Z materials is of general interest. First experimental works on this topic in low confinement scenarios of Tokamaks[10–14] and Stellarators[15] did not observe a significant variation of the impurity confinement with Z, using however quite a limited number of different materials.

Theoretical expectations for the impurity transport of different impurity species and impurity charges predict either a pronounced variation of the convective transport with Z or rather unaffected transport properties, depending on the respectively dominant transport mechanism, namely neoclassical[16,17] or turbulent transport[18]. Moreover, in non axis-symmetric devices, additional aspects as the existence of a mixed collisionality regime[19] or the build up of a radial electric field[20,21] are predicted by neoclassical theory and are expected to have impact on the impurity transport.

In this study, impurity transport properties have been investigated for a wide range of different impurity species within a stationary plasma scenario by measuring the impurity transport times τ_I[22,23] after pulsed impurity injections. After an introduction of the experimental method (section II), experimentally observed transport properties are discussed comparatively to theoretical expectations with respect to neoclassical and turbulent transport (section III).

II. EXPERIMENTAL METHOD

The stellarator W7-X is a magnetic confinement fusion device, designed for steady state plasma operation of up to 30 min under fusion relevant plasma conditions including neoclassical optimized particle confinement, minimized bootstrap currents and high beta values[24]. For an experimental determination of the global transport properties in W7-X, trace amounts of several different, non-recycling impurity species have been injected into stationary plasmas of constant heating power, temperature, and electron density. The injection of impurities has been realized using a laser blow-off (LBO) system[22] with a total amount of injected particles of less than 1×10^{18} particles as estimated by Wegner et al.[22], being non perturbative to the plasma temperature and density profiles. The signals of the highly ionized impurities, located well inside the bulk plasma, have been recorded

[a)] Electronic mail: andreas.langenberg@ipp.mpg.de

[b)] T. Klinger *et al.*, Nuclear Fusion **59**, 112004 (2019).

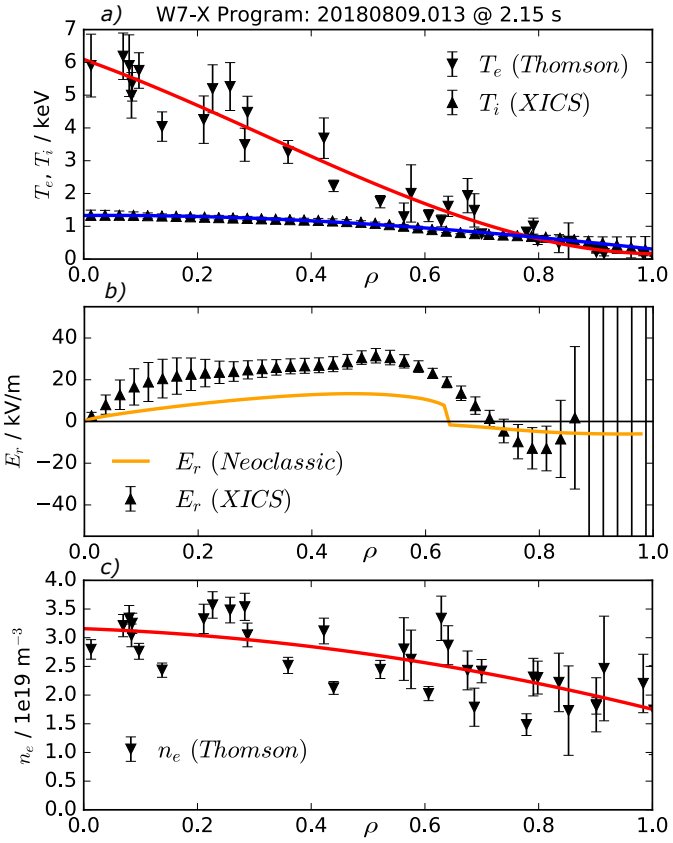

FIG. 1. a) Temperature, b) radial electric field, and c) density profiles as measured by the Thomson scattering (triangles down) and the XICS diagnostics (triangles up). Solid lines are fitted profiles, used as input for transport code calculations (see section IV).

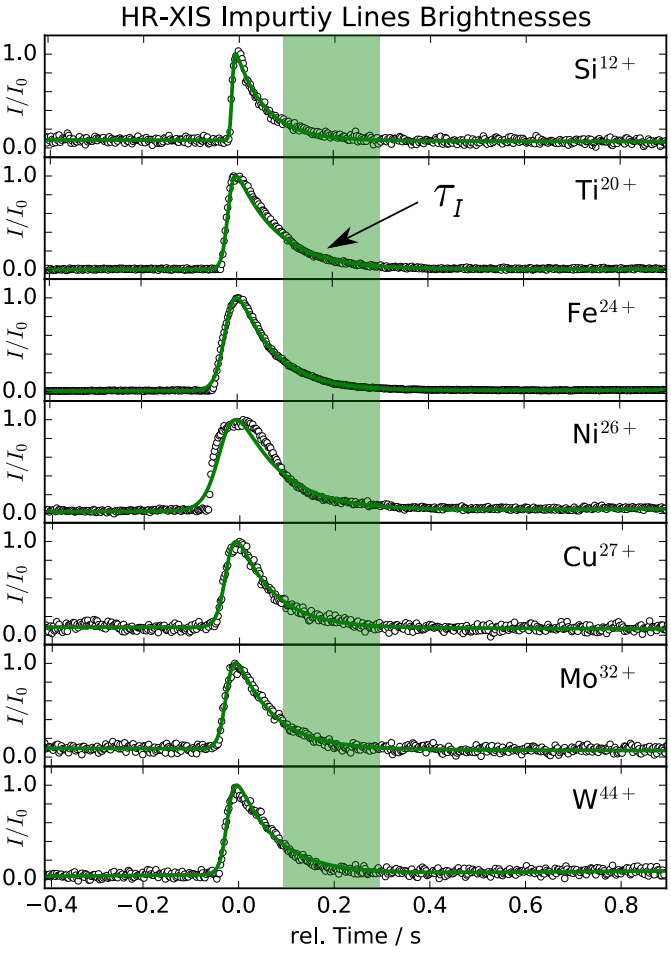

FIG. 2. Time traces for the brightness of several impurity species after pulsed impurity injections. The solid line corresponds to a fit of measured data (symbols), the shaded area was used for the τ_I determination.

making use of the high resolution X-ray imaging spectrometer (HR-XIS) and the X-ray imaging crystal spectrometer (XICS)[15], where XICS is used to measure T_i and E_r monitoring Ar impurities and HR-XIS is used to measure the injected impurity signals others than Ar. Alternatively, X-ray radiation from the injected impurities can also be observed by the pulse height analysis system (PHA), but with lower temporal resolution[25]. For each impurity species, identical plasma parameters have been reproduced and a separate experimental program was used for each impurity specie. All data shown in this work have been taken during the 3^{rd} experimental campaign of W7-X (OP1.2b)[26] in the magnetic standard configuration[27]. Plasma parameters have been chosen to obtain plasmas in the central electron root confinement (CERC) scenario, representing the majority of experimental programs from OP1.2b.

In Fig.1, measured temperature and density profiles of the repeated experiment programs are shown. As a consequence of the low electron density ($n_e = 3.2{\times}10^{19}\,m^{-3}$) and a pure electron heating using electron cyclotron resonance heating (ECRH)[28], all experiment programs in this study have been performed in CERC conditions with central T_e values being significantly larger than T_i (see Fig.1 a)), and a positive radial electric field E_r in the plasma center as measured by XICS in agreement with neoclassical predictions[20], see symbols and the solid line in Fig.1 b).

Fig.2 shows an overview of measured impurity signal time traces for all impurity species investigated in this study. Right after the injection, the impurity brightness shows a fast rise followed by an exponential decay. A fit of the exponential decaying impurity signal (shaded time interval in Fig.2) yields the impurity transport time τ_I being a direct measure of the global impurity confinement as discussed in detail elsewhere[22,23]. Since the HR-XIS and XICS data are functions of both, time and plasma radius ρ, defined as the square root of the normalized toroidal magnetic flux, in this study the ρ dependence of the impurity signal has been omitted by summing the detector counts over all viewing chords. For simulations of the impurity transport, the modeled signals shown in Fig.4 c) + d) have been derived from the volume integral of the calculated impurity densities. This reduction of ex-

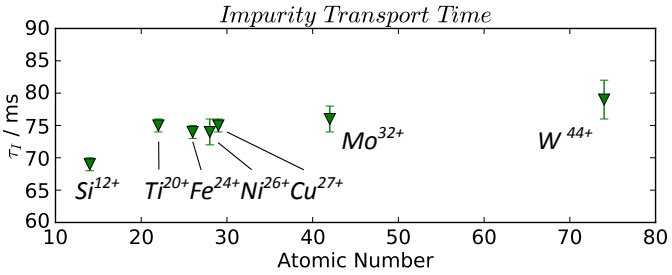

FIG. 3. Experimentally obtained impurity transport times τ_I for various atomic numbers of different atomic charges and charge to mass ratios of the impurity species.

perimental and theoretical data over ρ is well justified as impurity density profile shapes are expected to become stationary after a typical equilibration time[29] that for W7-X is in the order of 100 ms as shown in[15,22].

III. RESULTS AND DISCUSSION

A. Global Confinement for Different Impurity Species

In Fig.3, the experimentally derived impurity transport times τ_I for numerous impurities, namely silicon, titanium, iron, nickel, copper, molybdenum, and tungsten are shown. As can be seen, the measured τ_I values are very similar for a wide range of different impurities under the variation of the atomic number A as well as the atomic charge Z and the charge to mass ratio Z/M. In particular, although the impurity charge varies by about $\Delta Z = 55$ % going from Ti^{20+} to W^{44+}, the observed change in τ_I is only of $\Delta\tau_I = 6 \pm 2$ %. This shows at most a very weak dependence of impurity confinement for both the impurity charge and the impurity mass. This trend has also been observed in earlier studies at Alcator C-mod[10] and W7-X[15], although in those cases, the limited number of impurity species did not allow to draw any general conclusions on the Z and M dependence of impurity confinement so far.
It should be mentioned that despite the edge deposition of impurities using LBO, the injected impurities penetrate deep into the plasma core[30,31] and the observed τ_I values represent the bulk plasma properties and are not restricted to the plasma edge. This statement is supported by initial results from impurities deposited close to the plasma center using the TESPEL injection system[32], where also a similar trend of the above discussed weak Z and M dependence of τ_I has been observed[33].

B. Theoretical Expectations for Impurity Transport

In this section, theoretical predictions for neoclassical (including classical) impurity transport on the one hand and turbulence driven transport on the other hand are discussed comparatively and with respect to the experimental findings.
Models of neoclassical transport in the high collisionality regime ($\nu^* \gg 10^{-2}$, relevant to our experimental conditions) of highly charged impurities predict a pronounced Z dependence of the impurity convection velocity v and a charge and mass independent impurity diffusion D[16,17,19] with the former effect having a direct impact on the transport times τ_I.

$$\nu^* \gg 10^{-2} \Rightarrow D = const., v \propto Z \cdot E_r \qquad (1)$$

Here, the collisionality ν^* is defined according to[17] as

$$\nu^* = R_0 \nu_c / (\iota \tilde{v}) \qquad (2)$$

with the torus major radius R_0, the rotational transform on the magnetic axis ι, the particle speed $\tilde{v}$, and the collision frequency ν_c

$$\nu_c \propto \frac{n_e Z^2}{4\pi(\epsilon_0 M)^2}. \qquad (3)$$

In order to show the neoclassical expected τ_I to Z dependence explicitly for the experimental plasma conditions of this study, τ_I has been modeled using the one dimensional (magnetic flux surface averaged) transport code STRAHL[34]. As input parameters, the experimentally obtained T_e, T_i, and n_e profiles (solid lines in Fig.1) as well as the neoclassical expected E_r and the diffusive D and convective v transport parameter profiles, derived from the drift kinetic equation solver code DKES[35,36], have been used in the STRAHL modeling.
As the collision operator implemented in DKES is generally not valid at high collisionalities but the code is significantly cheaper with respect to computational time, the obtained DKES results have been cross validated exemplarily for Si^{12+} and W^{44+} impurities using the continuum drift-kinetic solver SFINCS[37–39], which implements the full linearized Fokker-Planck-Landau operator. As evident from Fig.4 a) and b), the DKES results for the D and v profiles (solid lines) compare reasonably well with the calculated SFINCS profiles shown in dashed lines. Therefore, throughout this work the DKES results have been used as STRAHL input parameters for the Si^{12+}, Ti^{20+}, Fe^{24+}, Ni^{26+}, Cu^{27+}, Mo^{32+}, and W^{44+} elements, considering classical as well as neoclassical transport.
The D profile shapes (Fig.4 a) are rather broad with a step like reduction at the radial position of the crossover of E_r from positive (electron root) to negative (ion-root) values, see Fig.1 b). Also the v profiles (Fig.4 b) exhibit a similar reduction at the E_r crossover, both effects also observed in other neoclassical transport studies[40,41] and in agreement with the shown profiles using SFINCS. We note that the neoclassical particle fluxes induced by the low D values are significantly smaller than those induced by v, *i.e.* the logarithmic impurity density gradient $d(ln(n_z))/dr$ must be of order 100 or larger for the diffusive transport to compare to the convective transport. At high collisionality, the neoclassical convection is not

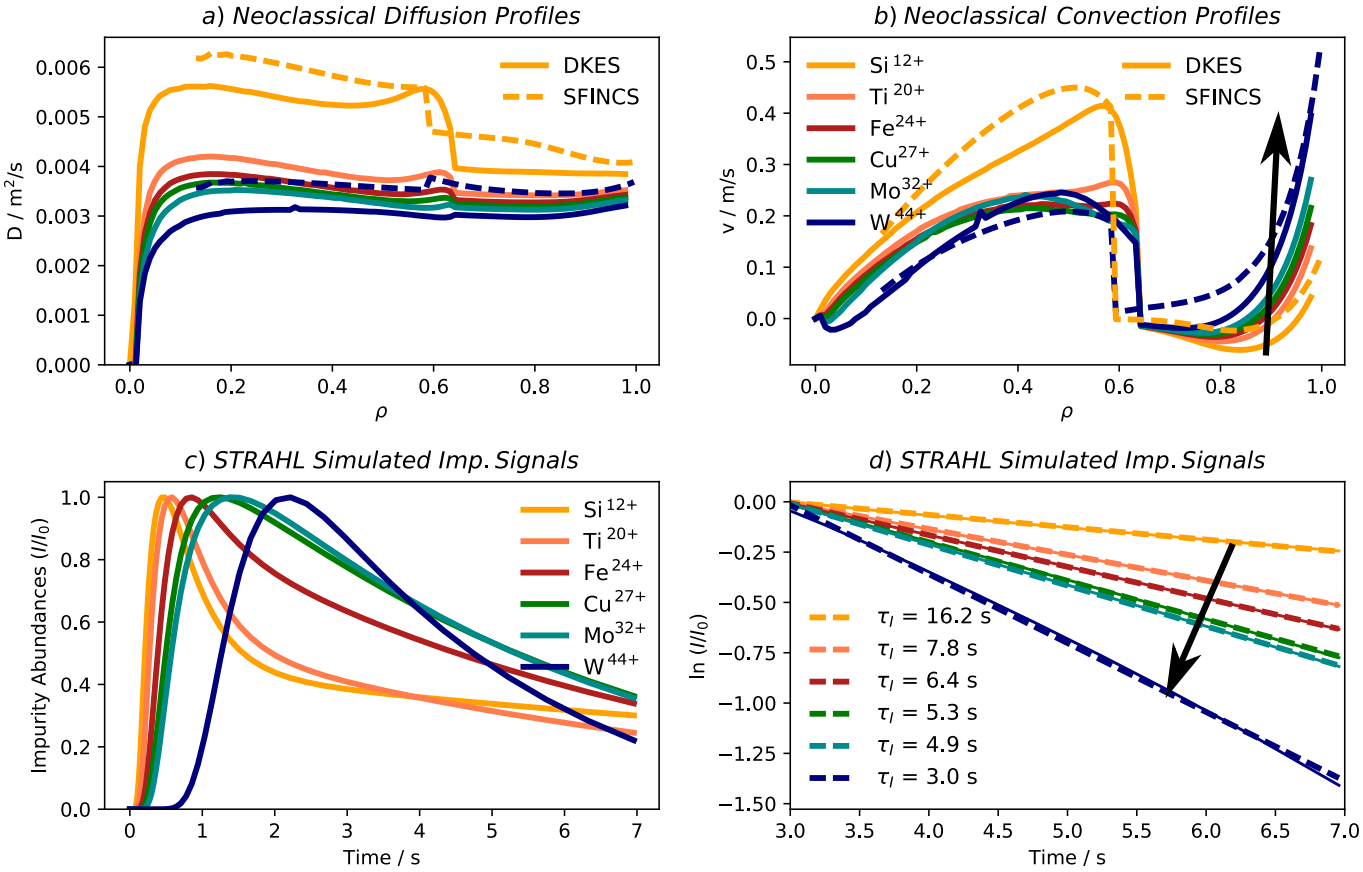

FIG. 4. a)+b) Neoclassical (including classical) expected D and v profiles for different impurity species shown in Fig.1 for a CERC plasma scenario. c)+d) Normalized STRAHL simulated time traces of different impurities species in a linear (c) and a logarithmic scale (d), together with modeled impurity transport times τ_I.

necessarily dominated by the radial electric field, and a lower Z impurity could experience a stronger convection than a higher Z impurity as seen in the plasma center. At the plasma edge, the v profiles exhibit higher positive (outward directed) convection velocities with higher Z, as expected from Equ.1. The convective transport is determined by an interplay between temperature screening and the drive from the main ion density gradient, as well as the relative size of the classical and neoclassical channel.

The modeled D and v profiles cause weaker confinement and shorter transport times τ_I of the high Z materials, evident from the STRAHL simulated time traces of the impurity signals shown in Fig.4 c)+d). Arrows on Fig.4 indicate the theoretical expected increasing v and decreasing τ_I with rising Z, as discussed above.

In Fig.5, the modeled τ_I values (dots) are shown together with those experimentally derived (triangles) for the different impurity species on a logarithmic scale. As can be seen, the experimental transport times do not follow the neoclassical expected trend of reduced confinement of higher Z materials, comparing the dashed lines in Fig.5. Even more striking, the experimental τ_I values undercut the theoretical ones up to a factor of about 100 in the case of Ti^{20+}. Both observations are in line with recent observations of large experimental diffusivities for Ar and Fe impurities in W7-X plasmas[30,40], hinting at a significant non-neoclassical impurity transport mechanism.

In fact, the observed marginal effect of the impurity mass and charge state on the transport properties of highly charged impurities is in agreement with theoretical predictions when impurity transport is dominated by turbulent diffusion[18]. In that case, a gyrokinetic model of quasilinear impurity transport yields a diffusion transport parameter D being independent of Z and M and which is dominant over the convective transport v. This predicted independence of D over Z and M is in line with the experimental observations shown in Fig.3+5: Here, τ_I is almost constant within the experimental uncertainties, despite a significant variation of Z=(12^+-44^+) as well as Z/M=(0.23-0.45).

IV. SUMMARY AND CONCLUSIONS

The experimental finding of a weak M and Z dependence of the transport time of highly charged impurities, theory[18] and direct measurements of impurity dif-

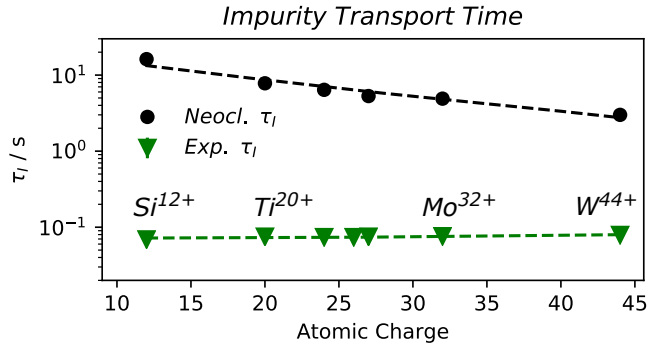

FIG. 5. Comparison of neoclassical expected and experimentally observed impurity transport times τ_I along Z for the impurity species shown in Fig.3.

fusion profiles[30,40] suggest that the impurity transport in W7-X is dominated by anomalous transport, being not inconsistent with theoretical expectations of turbulent transport[18,42]. The combination of weak Z dependence and high diffusivities is beneficial for avoiding impurity accumulation in long pulse operations of W7-X, especially for the high Z materials, including tungsten. So far, the Z dependence on impurity transport was systematically studied in low density, CERC plasmas but not yet under ion-root[20] and/or high density, high performance conditions[26,43]. Especially the latter ones exhibit an improved energy confinement for centrally peaked density profiles, that are expected to also impact the impurity confinement. Here, future experiments need to show the Z dependent transport under suppressed anomalous transport conditions, especially with respect to impurity accumulation scenarios on the envisaged experiment program time scales of several minutes.

V. ACKNOWLEDGMENTS

This work has been carried out within the framework of the EUROfusion Consortium and has received funding from the Euratom research and training programme 2014-2018 and 2019-2020 under grant agreement No 633053. The views and opinions expressed herein do not necessarily reflect those of the European Commission.
This scientific work was also partly supported by the Polish Ministry of Science and Higher Education within the framework of the scientific financial resources in the years 2014-2020 allocated for the realization of the international co-financed project.

[1] F. Effenberg, S. Brezinsek, Y. Feng, R. König, M. Krychowiak, M. Jakubowski, H. Niemann, V. Perseo, O. Schmitz, D. Zhang, *et al.*, Nuclear Fusion **59**, 106020 (2019).
[2] D. Zhang, R. König, Y. Feng, R. Burhenn, S. Brezinsek, M. Jakubowski, B. Buttenschön, H. Niemann, A. Pavone, M. Krychowiak, *et al.*, Phys. Rev. Lett. **123**, 025002 (2019).
[3] A. Kallenbach, M. Balden, R. Dux, T. Eich, C. Giroud, A. Huber, G. Maddison, M. Mayer, K. McCormick, R. Neu, *et al.*, Journal of Nuclear Materials **415**, S19 (2011), proceedings of the 19th International Conference on Plasma-Surface Interactions in Controlled Fusion.
[4] A. Dinklage, K. McCarthy, C. Suzuki, N. Tamura, T. Wegner, H. Yamada, J. Baldzuhn, K. Brunner, B. Buttenschön, H. Damm, *et al.*, Nuclear Fusion **59**, 076010 (2019).
[5] R. Burhenn, Y. Feng, K. Ida, H. Maassberg, K. McCarthy, D. Kalinina, M. Kobayashi, S. Morita, Y. Nakamura, H. Nozato, *et al.*, Nuclear Fusion **49**, 065005 (2009).
[6] Y. Nakamura, N. Tamura, M. Yoshinuma, C. Suzuki, S. Yoshimura, M. Kobayashi, M. Yokoyama, M. Nunami, M. Nakata, K. Nagaoka, *et al.*, Nuclear Fusion **57**, 056003 (2017).
[7] T. S. Pedersen, R. König, M. Jakubowski, M. Krychowiak, D. Gradic, C. Killer, H. Niemann, T. Szepesi, U. Wenzel, A. Ali, *et al.*, Nuclear Fusion **59**, 096014 (2019).
[8] C. P. Dhard, M. Mayer, S. Brezinsek, S. Masuzaki, G. Motojima, R. König, T. S. Pedersen, R. Neu, D. Hathiramani, M. Krause, *et al.*, Fusion Engineering and Design **146**, 242 (2019).
[9] M. Tokitani, S. Masuzaki, and T. Murase, Nuclear Materials and Energy **18**, 23 (2019).
[10] J. Rice, M. Reinke, C. Gao, N. Howard, M. Chilenski, L. Delgado-Aparicio, R. Granetz, M. Greenwald, A. Hubbard, J. Hughes, *et al.*, Nuclear Fusion **55**, 033014 (2015).
[11] M. Mattioli, C. D. Michelis, and A. Pecquet, Nuclear Fusion **38**, 1629 (1998).
[12] M. Mattioli, R. Giannella, R. Myrnas, C. Demichelis, B. Denne-Hinnov, T. D. D. Wit, and G. Magyar, Nuclear Fusion **35**, 1115 (1995).
[13] R. Giannella, L. Lauro-Taroni, M. Mattioli, B. Alper, B. Denne-Hinnov, G. Magyar, J. O. Rourke, and D. Pasini, Nuclear Fusion **34**, 1185 (1994).
[14] D. Pasini, R. Giannella, L. L. Taroni, M. Mattioli, B. Denne-Hinnov, N. Hawkes, G. Magyar, and H. Weisen, Plasma Physics and Controlled Fusion **34**, 677 (1992).
[15] A. Langenberg, N. A. Pablant, T. Wegner, P. Traverso, O. Marchuk, T. Bräuer, B. Geiger, G. Fuchert, S. Bozhenkov, E. Pasch, *et al.*, Review of Scientific Instruments **89**, 10G101 (2018), https://doi.org/10.1063/1.5036536.
[16] S. Buller, H. M. Smith, P. Helander, A. Mollen, S. L. Newton, and I. Pusztai, Journal of Plasma Physics **84**, 905840409 (2018).
[17] C. Beidler, K. Allmaier, M. Isaev, S. Kasilov, W. Kernbichler, G. Leitold, H. Maaßberg, D. Mikkelsen, S. Murakami, M. Schmidt, *et al.*, Nuclear Fusion **51**, 076001 (2011).
[18] P. Helander and A. Zocco, Plasma Physics and Controlled Fusion **60**, 084006 (2018).
[19] P. Helander, S. L. Newton, A. Mollén, and H. M. Smith, Phys. Rev. Lett. **118**, 155002 (2017).
[20] N. A. Pablant, A. Langenberg, A. Alonso, C. D. Beidler, M. Bitter, S. Bozhenkov, R. Burhenn, M. Beurskens, L. Delgado-Aparicio, A. Dinklage, *et al.*, Physics of Plasmas **25**, 022508 (2018), https://doi.org/10.1063/1.4999842.
[21] J. M. García-Regaña, T. Estrada, I. Calvo, J. L. Velasco, J. A. Alonso, D. Carralero, R. Kleiber, M. Landreman, A. Mollén, E. Sánchez, and C. Slaby, Plasma Physics and Controlled Fusion **60**, 104002 (2018).
[22] T. Wegner, B. Geiger, F. Kunkel, R. Burhenn, T. Schröder, C. Biedermann, B. Buttenschön, G. Cseh, P. Drews, O. Grulke, *et al.*, Review of Scientific Instruments **89**, 073505 (2018), https://doi.org/10.1063/1.5037543.
[23] A. Langenberg, F. Warmer, G. Fuchert, O. Marchuk, A. Dinklage, T. Wegner, J. A. Alonso, S. Bozhenkov, K. J. Brunner, R. Burhenn, *et al.*, Plasma Physics and Controlled Fusion **61**, 014030 (2019).
[24] J. Nührenberg, W. Lotz, P. Merkel, C. Nührenberg, U. Schwenn, E. Strumberger, and T. Hayashi, Fusion Technology **27**, 71 (1995), https://doi.org/10.13182/FST95-A11947048.
[25] M. Kubkowska, A. Czarnecka, T. Fornal, M. Gruca, S. Jabłoński, N. Krawczyk, L. Ryć, R. Burhenn, B. Buttenschön, B. Geiger, *et al.*, Review of Scientific Instruments **89**, 10F111 (2018), https://doi.org/10.1063/1.5038850.

[26]R. C. Wolf, A. Alonso, S. Äkäslompolo, J. Baldzuhn, M. Beurskens, C. D. Beidler, C. Biedermann, H.-S. Bosch, S. Bozhenkov, R. Brakel, *et al.*, Physics of Plasmas **26**, 082504 (2019), https://doi.org/10.1063/1.5098761.
[27]T. Andreeva, "Vacuum magnetic configurations of wendelstein 7-x," Tech. Rep. (Max-Planck-Institut für Plasmaphysik, Garching, 2002).
[28]R. C. Wolf, S. Bozhenkov, A. Dinklage, G. Fuchert, Y. O. Kazakov, H. P. Laqua, S. Marsen, N. B. Marushchenko, T. Stange, M. Zanini, *et al.*, Plasma Physics and Controlled Fusion **61**, 014037 (2018).
[29]G. Fussmann, Nuclear Fusion **26**, 983 (1986).
[30]A. Langenberg, N. Pablant, O. Marchuk, D. Zhang, J. Alonso, R. Burhenn, J. Svensson, P. Valson, D. Gates, M. Beurskens, *et al.*, Nuclear Fusion **57**, 086013 (2017).
[31]A. Langenberg, J. Svensson, O. Marchuk, G. Fuchert, S. Bozhenkov, H. Damm, E. Pasch, A. Pavone, H. Thomsen, N. A. Pablant, *et al.*, Review of Scientific Instruments **90**, 063505 (2019), https://doi.org/10.1063/1.5086283.
[32]R. Bussiahn, N. Tamura, K. J. McCarthy, R. Burhenn, H. Hayashi, R. Laube, and T. Klinger, Review of Scientific Instruments **89**, 10K112 (2018), https://doi.org/10.1063/1.5038844.
[33]M. Kubkowska, N. Tamura, A. Chomiczewska, T. Fornal, M. Gruca, N. Krawczyk, S. Jablonski, L. Ryc, R. Bussiahn, K.-J. Brunner, *et al.*, Journal of Instrumentation **15** (2020), doi: 10.1088/1748-0221/15/01/C01019.
[34]R. Dux, *STRAHL user manual*, Max-Planck-Institue for Plasmaphysics (2006), IPP Report 10/30.
[35]S. P. Hirshman, K. C. Shaing, W. I. van Rij, C. O. Beasley, and E. C. Crume, The Physics of Fluids **29**, 2951 (1986), https://aip.scitation.org/doi/pdf/10.1063/1.865495.
[36]W. I. van Rij and S. P. Hirshman, Physics of Fluids B: Plasma Physics **1**, 563 (1989), https://doi.org/10.1063/1.859116.
[37]M. Landreman, H. M. Smith, A. Mollén, and P. Helander, Physics of Plasmas **21**, 042503 (2014), https://doi.org/10.1063/1.4870077.
[38]A. Mollén, M. Landreman, and H. M. Smith, Journal of Physics: Conference Series **561**, 012012 (2014).
[39]A. Mollén, M. Landreman, H. M. Smith, J. M. García-Regaña, and M. Nunami, Plasma Physics and Controlled Fusion **60**, 084001 (2018).
[40]B. Geiger, T. Wegner, C. Beidler, R. Burhenn, B. Buttenschön, R. Dux, A. Langenberg, N. Pablant, T. Pütterich, Y. Turkin, *et al.*, Nuclear Fusion **59**, 046009 (2019).
[41]Y. Turkin, C. D. Beidler, H. Maassberg, S. Murakami, V. Tribaldos, and A. Wakasa, Physics of Plasmas **18**, 022505 (2011).
[42]T. Wegner, B. Geiger, J. A. Alcuson, P. Xanthopoulos, R. Burhenn, F. Kunkel, C. Agnioni, M. Beurskens, L.-G. Böttger, S. Bozhenkov, *et al.*, (2019), Submitted for publication.
[43]S. A. Bozhenkov, Y. Kazakov, O. Ford, M. N. A. Beurskens, J. A. Alcuson, J. A. Alonso, J. Baldzuhn, C. Brandt, K. J. Brunner, H. Damm, *et al.*, Nuclear Fusion (2020).